**PAPER**

# Effect of indium doping on motions of $\langle a \rangle$-prismatic edge dislocations in wurtzite gallium nitride

To cite this article: Cheng Chen *et al* 2019 *J. Phys.: Condens. Matter* **31** 315701

View the article online for updates and enhancements.

# Effect of indium doping on motions of ⟨*a*⟩-prismatic edge dislocations in wurtzite gallium nitride

**Cheng Chen**[1] , **Fanchao Meng**[1], **Pengfei Ou**[1] , **Guoqiang Lan**[1], **Bing Li**[2], **Huicong Chen**[1], **Qiwen Qiu**[1] **and Jun Song**[1,3]

[1] Department of Materials Engineering, McGill University, Montréal, Québec H3A0C5, Canada
[2] School of Engineering, Huzhou University, Huzhou 313000, People's Republic of China

E-mail: jun.song2@mcgill.ca

## Abstract

The influences of indium doping on dynamics of ⟨*a*⟩-prismatic edge dislocation along $(1\,\bar{1}\,0\,0)\,[1\,1\,\bar{2}\,0]$ shuffle plane in wurtzite GaN have been investigated employing classical molecular dynamics (MD) simulations. The dependence of dislocation motion mode and dislocation velocity on indium doping concentration, temperature, and applied shear stress was clarified. Moreover, the simulation results were further analyzed using elastic theory of dislocation and thermal activation theory of dislocation motion, showing excellent agreement with the simulation. Our findings help gain deep insights into modifying dynamic behaviors of TDs through the alloying doping and offer generic tools to the study of other wurtzite materials of promising application prospects, such as AlGaN and ZnO.

Keywords: dislocation, mobility, InGaN, molecular dynamics, doping

S Supplementary material for this article is available online

(Some figures may appear in colour only in the online journal)

## 1. Introduction

Due to the unique capacities in tailoring the band gap, GaN-based materials e.g. InGaN and AlGaN, have been extensively used in electronic devices including power electronics, highly-efficient light-emitting optoelectronics, UV detectors, etc [1–14]. However, the performance and lifetime of GaN-based devices have been severely threatened by the presence of high densities of dislocations generated during the crystal growth of GaN [15–18]. Therefore, significant effort has been and is being spent in developing newer techniques that suppress the generation of dislocations during GaN production, including but not limited to chemical exfoliation, [19] growing buffer layers [20], epitaxial lateral overgrowth [5, 21–25], dislocation filtering based on selective area growth [26] and ammonothermal techniques [27].

However, to-date, fundamental understanding of dislocation dynamics in GaN remains rather limited, which is in stark contrast to tremendous advances on the studies of the optoelectronic properties of GaN-based materials. This is manly attributed to the complexity of wurtzite hexagonal crystal symmetry containing multiple slip systems (basal, prismatic and pyramidal) and the diverse and rich dislocation core structures such as, *a*-type edge, *c*-type screw, and (*a* + *c*)-type mixed dislocations [28–32]. To date, only the dynamics of *a*-type edge and *c*-type screw dislocations have been examined in pristine GaN [31, 33, 34].

Moreover, the interplay between alloying elements (e.g. In, Al) with dislocations in GaN is poorly understood. Given the significant role of alloying in modulating the electrical and optical properties of GaN-based devices, further research efforts are necessary to address such knowledge deficit in order to achieve targeted defect engineering and property tuning. The knowledge would also be essential for the design

[3] Author to whom correspondence should be addressed.
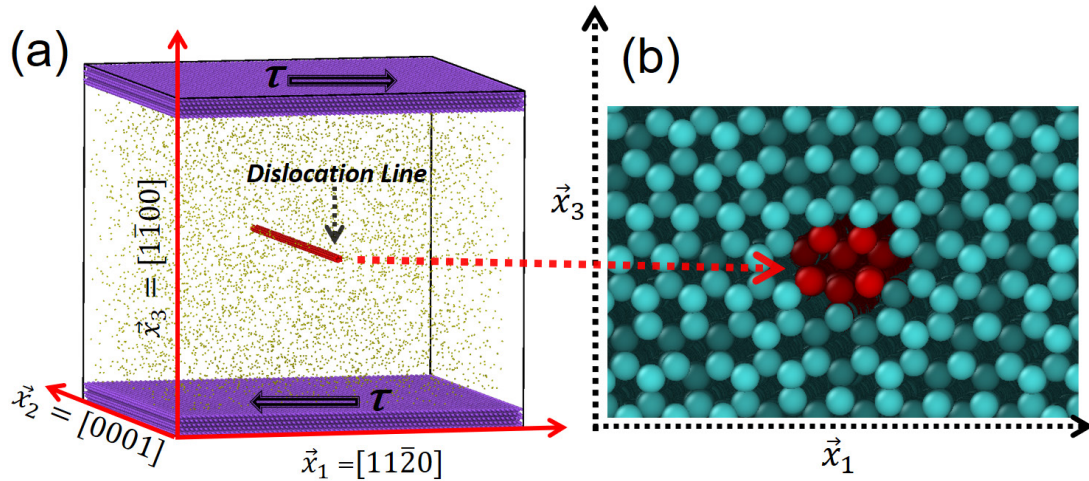
**Figure 1.** (a) Illustration of the simulation supercell wherein the alloying In atoms are colored yellow, introduced via random substitution of the Ga atoms. The top and bottom slabs of atoms where shear stresses are applied to drive dislocation motions, are colored in purple, while atoms in the dislocation core are colored red. The other lattice Ga and N atoms are not shown for clarity. (b) An enlarged projection view along $\vec{x}_2$ depicting the dislocation core structure.

and development of the (In, Al)GaN coatings, whose mechanical performance, e.g. wear resistance, is directly related to dislocation dynamics therein [35, 36].

The present study focuses on the influence of the common alloying element, indium (In), on dislocation dynamics in GaN. It has been demonstrated experimentally that under normal growth conditions, *a*-type edge dislocations having the smallest Burger's vector on the prismatic slip system are the main contributor to the high dislocation density in growing GaN crystal, because of the less lattice distortion and relatively lower stress required to move a dislocation [37–39]. Therefore, in this paper, the $\langle a \rangle$-prismatic edge dislocation along $\left(1\ \bar{1}\ 0\ 0\right)\left[1\ 1\ \bar{2}\ 0\right]$ shuffle plane has been chosen as the representative example. Employing large-scale atomistic simulations, we systematically examined the dislocation motions in In-doped GaN. The effects of In alloying on the threshold stress and displacement mode of the dislocation have been examined, and further analyzed using in the framework of continuum mechanics. Meanwhile, the influence of In alloying on the evolution of dislocation velocity as the shear stress and temperature vary has been examined, and the role of In alloying on the activation energy barrier and activation volume has been assessed. Our findings provide essential information on understanding the dynamic behaviors of dislocations in impurity-doped GaN.

## 2. Computational methodology

Classical molecular dynamics (MD) simulations were performed using the LAMMPS package [40]. On base of the hexagonal wurtzite GaN unit cell, a rectangular dislocation containing supercell was constructed with three orthonormal vectors $\vec{x}_1$ parallel to the Burgers vector $\vec{b} = 1/3\left[1\ 1\ \bar{2}\ 0\right]$, $\vec{x}_2$ along $[0\ 0\ 0\ 1]$ and $\vec{x}_3$ normal to the glide plane $\left(1\ \bar{1}\ 0\ 0\right)$. In the context below, we denote *b* as the magnitude of the Burgers vector $\vec{b}$. The *a*-type edge dislocation on the prismatic plane

$\left(1\ \bar{1}\ 0\ 0\right)$ was introduced at the center of the supercell, with its location and core configuration illustrated in figure 1. The initial dislocation structure was generated by displacing atoms in the simulation supercell according to isotropic linear elasticity theory, as detailed in several previous studies [41, 42]. The supercell has free boundary condition along $\vec{x}_3$, while periodic along $\vec{x}_1$ and $\vec{x}_2$, which coincide with the dislocation line and Burgers vector directions respectively. It is of dimensions 25.49 nm × 22.31 nm × 23.56 nm along $\vec{x}_1$, $\vec{x}_2$ and $\vec{x}_3$ directions respectively and contains a total of 1144 890 atoms. Benchmark calculations have been performed to verify that the supercell dimensions are sufficiently large to eliminate the influence of image dislocation–dislocation interactions on the simulation results. The solute In atoms were introduced by randomly substituting Ga atoms in the lattice according to the desired concentration.

The interatomic interactions of the In–Ga–N system are described by the the Stillinger-Weber [43] potential developed by Zhou *et al* [44]. This potential has been demonstrated to correctly predict key physical properties, including the crystal structure, lattice constant, elastic moduli, and defect characteristics for the ternary system In–Ga–N [45] under stoichiometric conditions, and has been previously used to study strain relaxation of misfit dislocations [46, 47], heteroepitaxial growth [48] and substitutional diffusion [45].

After the construction of the simulation supercell and dislocation, the system was first relaxed via energy minimization followed by relaxation in the isothermal–isobaric (NPT) ensemble [49, 50] for 10 ns till the steady state of zero pressure condition (along periodic directions) and constant temperature is achieved. The simulation duration after the application of the shear stress was ~1 ns or till the overall dislocation displacement was beyond 200 nm. The damping parameters used for temperature and pressure controls are 0.1 and 1 respectively. It is worth mentioning that the choice of damping parameters (in suitable ranges) will only affect the equilibration time and the magnitude/frequency of thermal fluctuation, but not alter

the results or conclusions. The timestep of one femtosecond (fs) has been set for all simulations. Then the shear stress was imposed on the material through applying equal but opposite forces to atoms in the top and bottom slabs, each of 3 nm in thickness (see figure 1), to drive the dislocation to move. The temperature and In concentration ranges considered in the present study are (800 K–1100 K) and (0–0.18) respectively. The temperature range of 800 K–1000 K was chosen mainly because it is in accordance with the typical temperature range for the growth of GaN and GaN-based heterostructures [51–53]. Meanwhile this temperature range would provide sufficient thermal activation for dislocation motions. The In concentration range examined in this study is 0–0.18 (atomic percentage). However we focus on a narrow concentration range of (0–0.05) when investigating dislocation mobility because we would like to stay in (relatively) dilute limit but at the same time be able to observe apparent solute effect.

The dislocation motion was monitored by examining its displacement under different applied shear stresses as a function of the simulation time. The position of dislocation at a particular instant of time was obtained through averaging the coordinates of disordered core atoms along the dislocation line direction.

## 3. Results and discussion

### 3.1. Effect of In alloying on modes of dislocation motions

First we examined the stress-driven dislocation motions in the pristine GaN without In alloying, for which figure 2 presents a representative set of results showing the displacement of the dislocation as a function of the simulation time under different applied shear stresses, at $T = 1000$ K. Continuous displacement of dislocations was observed to initiate once the applied stress goes beyond a threshold stress $\sigma_{th}^0 \cong 0.1$ GPa. As the stress continues to increase, dislocation motions are accelerated. However, the evolution of dislocation displacement follows two different patterns, being (*i*) the step-wise increment at relative small stresses and (*ii*) approximately linear increment at high stresses, as the simulation time increases. Detailed examination of the dislocation movement shows that these two patterns directly correspond to two distinct modes of dislocation motions. As illustrated in figure 3(a), the step-wise displacement is attributed to the kink-like motion of dislocation, controlled by the trapping/de-trapping of local dislocation segment, while the linear displacement at high stresses corresponds to the dislocation staying more or less as a straight dislocation and moving as a whole, as shown in figure 3(b) (for further details please see supplementary materials (stacks.iop.org/JPhysCM/31/315701/mmedia))

With In alloying, same scenarios of dislocation behaviors were observed. However, it is found that In alloying tends to inhibit dislocation motions, rendering the need of higher stresses not only to initiate dislocation motions but also for the change from kink-like motion to linear straight dislocation displacement, as can be seen from figures 2(b) and (c). Examining the threshold stress required to initiate dislocation
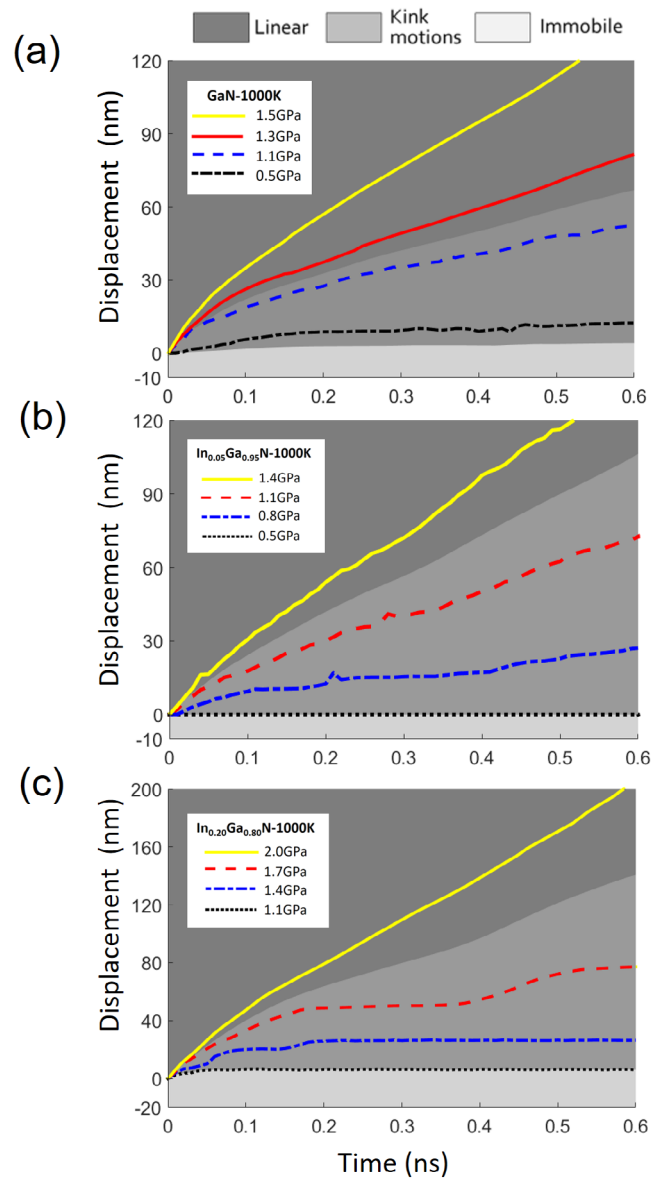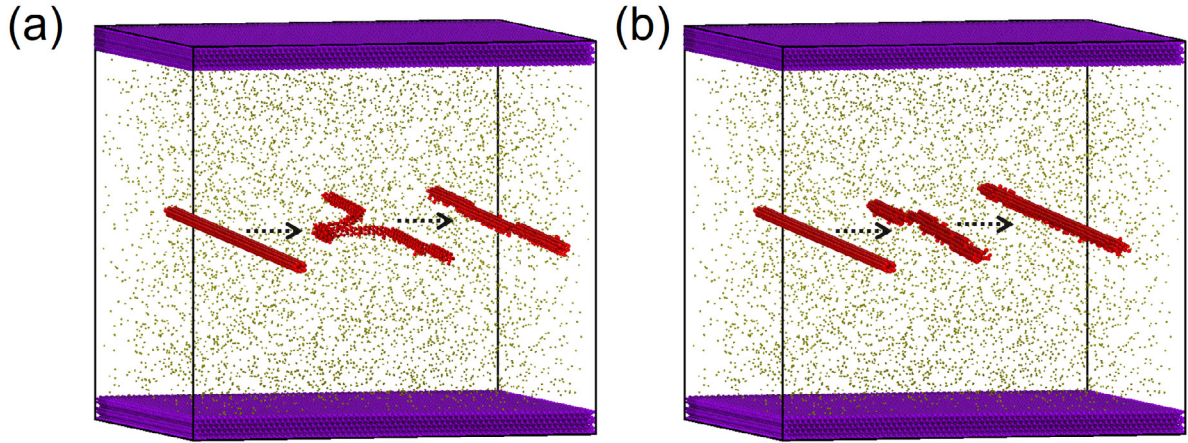


**Figure 2.** The time evolution of dislocation displacement under different applied shear stresses and $T = 1000$ K for (a) pristine GaN and GaN systems with In concentration of (b) $c_{In} = 0.05$ and (c) $c_{In} = 0.2$. The different shaded regions indicate different modes of dislocation motions.

motions, thereafter denoted as (and $\sigma_{th}^0$ for pristine GaN), as a function of the In alloying concentration in figure 4(a), we see that $\sigma_{th}$ is linearly proportional to the In concentration. Such concentration dependence can be understood from continuum mechanics and quantitatively evaluated by calculating the extra stress the dislocation core needs to overcome the local lattice distortion induced by the randomly distributed In atoms, as elaborated in the follows

The stress field of an edge dislocation is [54]

$$\sigma_{x_1} = -\frac{Gbx_3}{2\pi(1-\nu)}\frac{3x_1^2 + x_3^2}{x_1^2 + x_3^2} \tag{1}$$

$$\sigma_{x_3} = -\frac{Gbx_3}{2\pi(1-\nu)}\frac{x_1^2 - x_3^2}{x_1^2 + x_3^2} \tag{2}$$

**Figure 3.** Evolution of dislocation structures, from MD simulations, when the dislocation displacement exhibits (a) a step-wise increment, induced by the kink-like dislocation motions associated with the trapping/de-trapping of local dislocation segment, and (b) linear increment with the dislocation line being mostly straight.
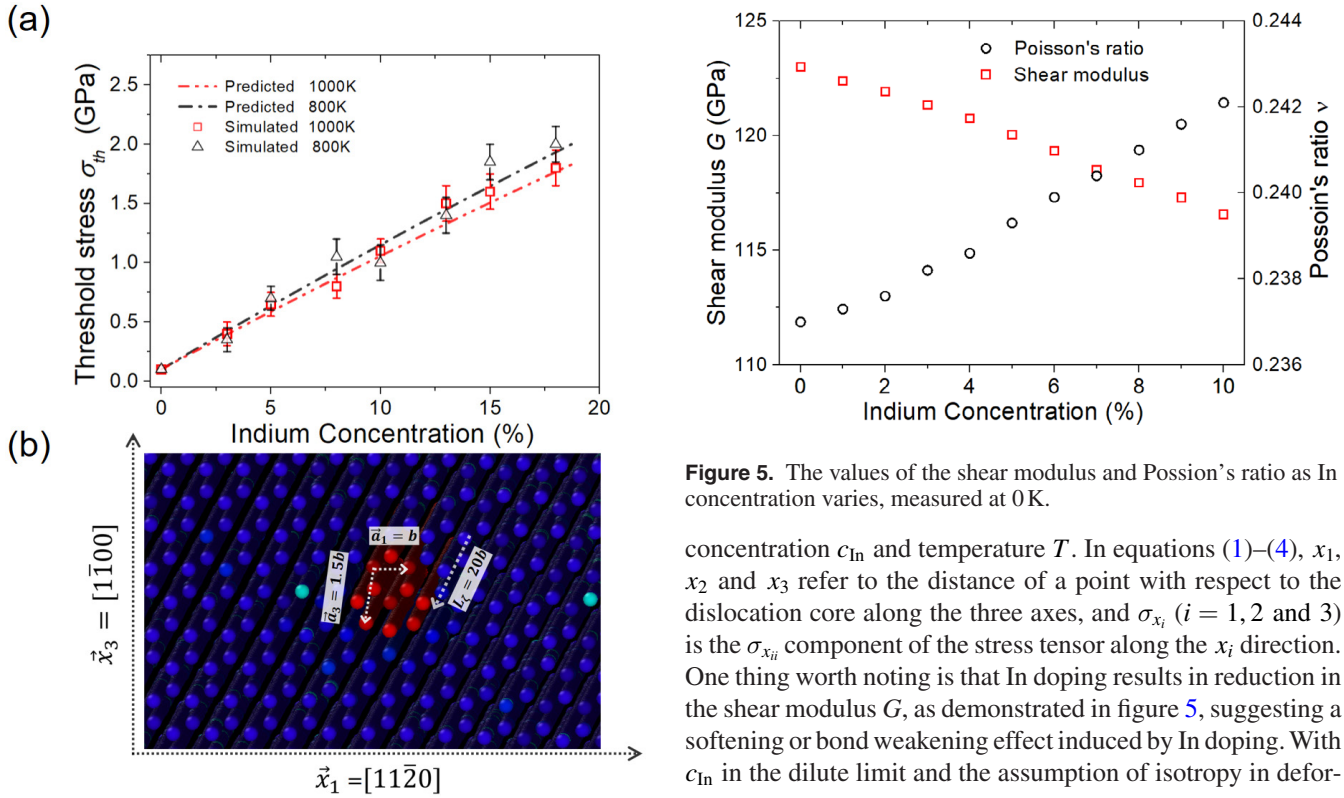


**Figure 4.** (a) The threshold stress $\sigma_{th}$ required to initiate dislocation motions as a function of $c_{In}$ obtained from MD simulations and predicted from equation (5) at $T = 800$ K and $T = 1000$ K. (b) The local distorted geometry that the *a*-type edge dislocation needs to overcome.

$$\sigma_{x_2} = v \left( \sigma_{x_1} + \sigma_{x_3} \right). \tag{3}$$

Therefore, the effective pressure on a volume element $\Omega$ is

$$\sigma_p = \frac{Gb(1+\nu)}{3\pi(1-\nu)} \frac{x_3}{x_1^2 + x_3^2}. \tag{4}$$

Where, $\nu$ and $G$ represent Poisson's ratio and shear modulus of the material system, respectively, depending on indium doping



**Figure 5.** The values of the shear modulus and Possion's ratio as In concentration varies, measured at 0 K.

concentration $c_{In}$ and temperature $T$. In equations (1)–(4), $x_1$, $x_2$ and $x_3$ refer to the distance of a point with respect to the dislocation core along the three axes, and $\sigma_{x_i}$ ($i = 1, 2$ and 3) is the $\sigma_{x_{ii}}$ component of the stress tensor along the $x_i$ direction. One thing worth noting is that In doping results in reduction in the shear modulus $G$, as demonstrated in figure 5, suggesting a softening or bond weakening effect induced by In doping. With $c_{In}$ in the dilute limit and the assumption of isotropy in deformation, the average lattice distortion $\varepsilon$ can be approximated as $\frac{a_{InN} - a_{GaN}}{a_{GaN}} \cdot c_{In}$ with $a_{InN} = 3.517$ Å and $a_{GaN} = 3.175$ Å being the lattice constants (at $T = 0$ K) of wurtzite InN and GaN along $\vec{x}_1$ direction respectively. In the above, the solute-induced lattice distortion was assumed to be isotropic. The validity of this isotropic assumption was confirmed by examining the elastic dipole field $P_{ij}$ of an isolated In solute in the GaN matrix (see supplementary materials for details). Then threshold stress required to initiate dislocation displacement in the case of In doping can then be derived as

$$\sigma_{th} = \max \left[ \frac{1}{b^2} \mathrm{d} \left( \varepsilon \sigma_p \Omega \right) / \mathrm{d} x_1 \right] + \sigma_{th}^0 \tag{5}$$

where $\Omega$ denotes the minimum distortion volume the dislocation needs to overcome and can be estimated as $\Omega = L_\zeta \cdot \vec{a}_1 \cdot \vec{a}_3$

[41], where $L_\zeta = 20b$ is the dislocation line length $|\vec{a}_1|$ and $|\vec{a}_2|$, as illustrated in figure 4(b), are fitted to be $b$ and $1.5b$ respectively, based on the simulated results. The predicted $\sigma_{th}$ as a function of the In concentration is shown in figure 4(a), in comparison with the simulation data, and we can see that a good agreement has been achieved.

### 3.2. The effects of indium on dislocation velocity

Based on the displacement versus simulation time curves in figure 2, the dislocation velocity can be extracted. However, considering the uncertainty and randomness of the kinks motion of dislocation, we only focus on the linear motion mode of dislocation. Doping concertation $c_{In} \in (0\text{--}0.05)$ and the applied stress $\tau > 1$ GPa was used to obtain reliable evaluation about the steady-state dislocation velocity. Figure 6 shows the velocity of edge dislocation $v_d$ as a function of applied shear stress $\tau$ at different In concentrations and $T = 800$ K, 900 K and 1100 K.(see Supplementary Materials for further details of error analysis) It can be observed that the dislocation velocity shows an increasing trend with the increase of stress and temperature, which reveals the thermally activated mechanisms of dislocation motion. However, there is a noticeable contrast between the pristine GaN and In-doped GaN in terms of the velocity evolution. From figure 6, we see that for the pristine GaN, $\ln(v_d)$ exhibits a linear trend as the shear stress $\tau$ increases, while In doping leads to apparent deviation from this linear trend. Compared to the case of pristine GaN, it is observed that In doping facilitates dislocation motions at low dislocation velocities, but impedes dislocation motions at high velocities. Such stress-dependent effect of In doping may be attributed to competition between the In doping induced softening or bond weakening effect (see figure 5) which facilitates dislocation slip in low-velocity regime, and the impedance from the local volume distortion and drag effect of In with larger atomic mass, which grows as the velocity increases and becomes dominant at large stresses. Moreover, we see that the degree of impedance due to In induced volume distortion and drag in the high-stress regime is proportional to $c_{In}$.

The velocity $v_d$ of $a$-type edge dislocation is further analyzed using the empirical Arrhenius relationship [41, 54]:

$$v_d = v_0 \exp\left(-\frac{\Delta Q - \tau\Phi}{kT}\right) \qquad (6)$$

where $Q$ is the activation energy barrier, $\Phi$ is the activation volume at increased $c_{In}$, $k$ denotes Boltzmann's constant, $T$ is the temperature, and $v_0$ represents the barrierless velocity of dislocation. The obtained velocity as a function of applied shear stress at different temperature for different doping concentrations are plotted in figure 7, and the fitted energy barrier $Q$ and activation volume $\Phi$ are listed in the table 1. We see that $\Phi$ and $\Delta Q$ exhibit an overall decreasing trend with the increase of $c_{In}$, suggesting that the doped indium atoms facilitate the dislocation slip. This is consistent with our previous analysis that In doping accelerates dislocation motions in the low shear stress regime before the drag effect kicks in. We also searched the related studies and to-date, only the dynamics of prismatic
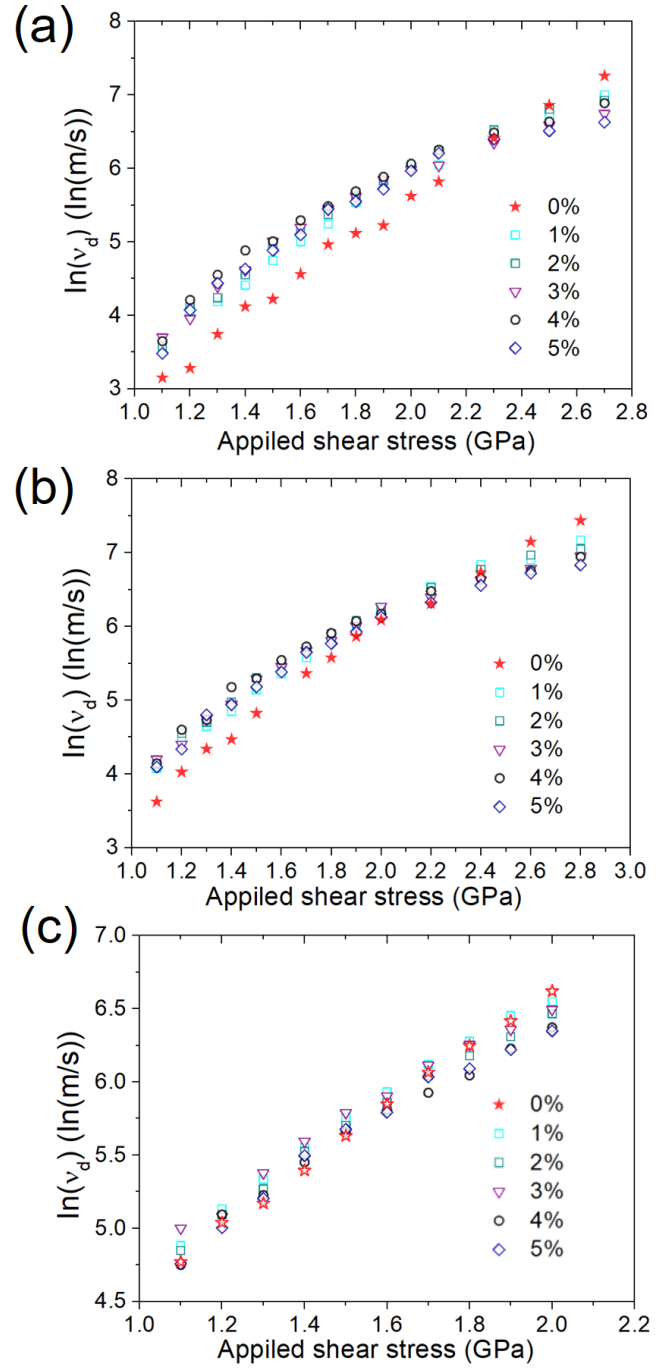


**Figure 6.** The evolution of dislocation velocity as a function of the applied shear stress $\tau$ at different In doping concentration $c_{In}$ at (a) $T = 800$ K, (b) $T = 900$ K, and (c) $T = 1100$ K. An error analysis of the dislocation velocity has also been performed (see details in supplementary materials).

$a$-type edge dislocations have been examined in pristine GaN using a Tersoff-like potential by Weingarten *et al* [34] However, the dislocation velocity found here is supersonic and much larger than those found in previous works [34], possibly because of a different ternary In–Ga–N Stillinger–Weber (SW) potential used in this work. It is worth noting that the Tersoff-like potential developed for the pristine GaN [55] is usually more reliable and transferable than the SW one, providing even much lower dislocation velocities.
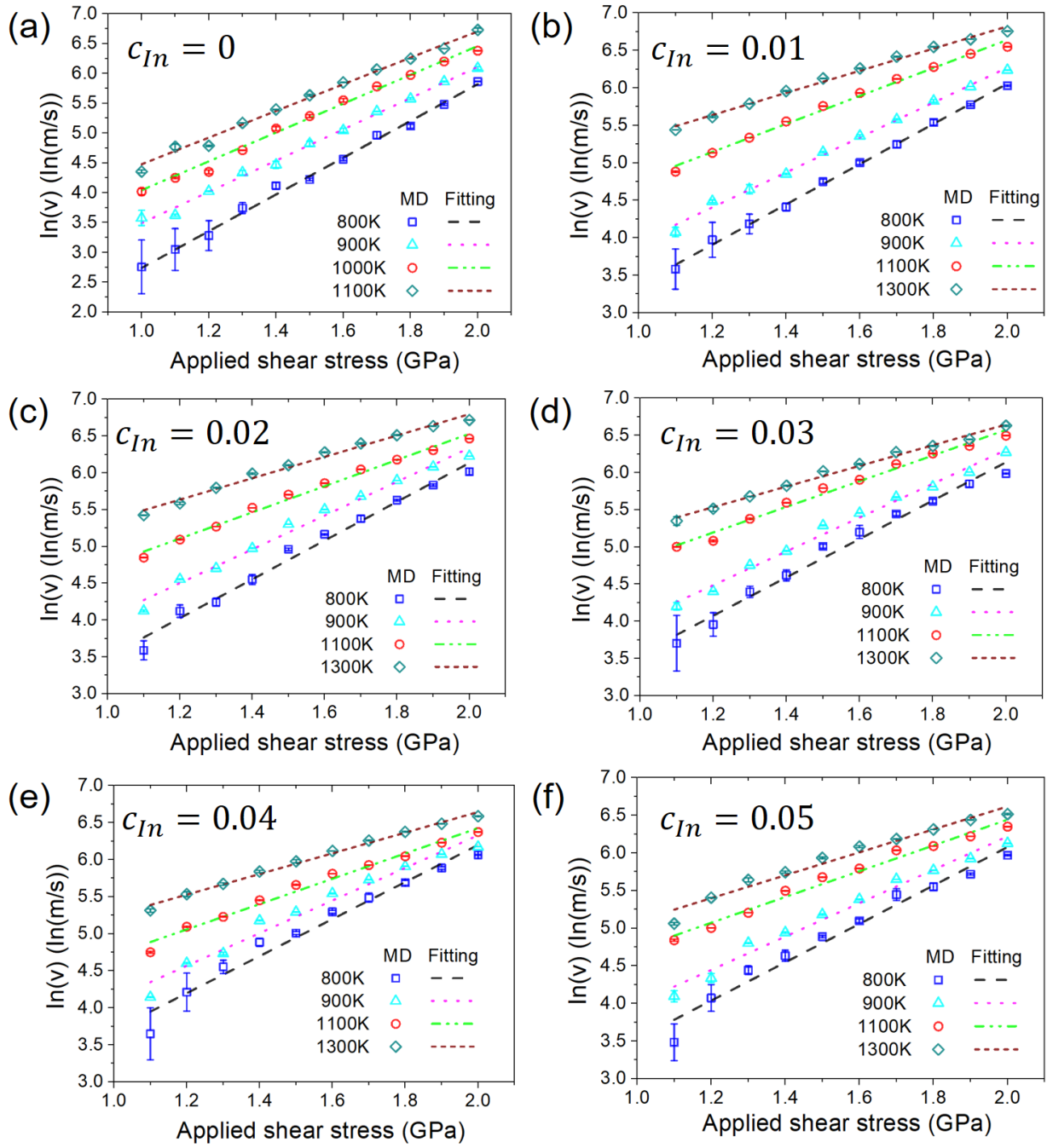
**Figure 7.** Arrhenius relationships between the dislocation velocity and temperature ($T = 800 \sim 1300$ K) at increased In doping concentrations: (a) $C_{In} = 0$, (b) $C_{In} = 0.01$, (c) $C_{In} = 0.02$, (d) $C_{In} = 0.03$, (e) $C_{In} = 0.04$, (f) $C_{In} = 0.05$ (see details regarding the error analysis in the supplementary materials).

**Table 1.** The values of energy barrier $Q$ and activation volume $\Phi$ obtained via fitting using data in figure 7 for different $c_{In}$ (see the corresponding $\ln(v)$ versus $-1/T$ plots in supplementary materials).

| $c_{In}$ (atm%) | 0 | 0.01 | 0.02 | 0.03 | 0.04 | 0.05 |
|---|---|---|---|---|---|---|
| $\Phi$ (Å$^3$) | $33.4 \pm 0.5$ | $28.4 \pm 0.9$ | $27.7 \pm 0.8$ | $27.0 \pm 1.0$ | $26.5 \pm 0.7$ | $27.3 \pm 0.6$ |
| $\Delta Q$ (eV) | $0.67 \pm 0.01$ | $0.54 \pm 0.01$ | $0.52 \pm 0.02$ | $0.48 \pm 0.02$ | $0.47 \pm 0.03$ | $0.48 \pm 0.02$ |

## 4. Conclusion

In summary, the effects of In doping on dynamics of the $\langle a \rangle$-prismatic edge dislocation along the shuffle plane of $(1\ \bar{1}\ 0\ 0)\ [1\ 1\ \bar{2}\ 0]$ in GaN were studied using molecular dynamics (MD) simulations. Under the application of shear stress, the dislocation motion is found to exhibit two distinct modes, being the kink-like and linear motions in low-stress and high-stress regimes respectively. The threshold shear stresses to induce these two modes are found to increase as the In concentration increases. In particular, the In-induced increase in the lower threshold stress to initiate the (kink-like) dislocation motion was attributed to the need of the dislocation to overcome the local lattice distortion caused by In alloying, which can be quantitatively evaluated through continuum dislocation theory. For linear motions of dislocations, examining the evolution of velocity as a function of the shear stress, we found that In alloying has two competing effects, being bond weakening to reduce the lattice resistance, and the impedance from local volume distortion and drag effect due to the larger atomic mass of In. It was observed that the bond weakening effect prevails to facilitate dislocation motions at low velocities, while the impedance due to volume distortion and drag dominates at high velocities. Such competition results in different stress-dependence of dislocation velocity in In-doped and pristine GaN. Moreover, In alloying was found to reduce both the activation energy barrier and activation volume. The present study provides essential information towards understanding the role of alloying in modifying the dynamics and evolution of dislocations in GaN.

## Acknowledgment

## ORCID iDs

Cheng Chen ⬡ https://orcid.org/0000-0003-3062-9048
Pengfei Ou ⬡ https://orcid.org/0000-0002-3630-0385

## References

[1] Belabbas I, Nouet G and Komninou P 2007 *J. Cryst. Growth* **300** 212
[2] Cho C Y, Kwon M K, Park I K, Hong S H, Kim J J, Park S E, Kim S T and Park S J 2011 *Opt. Express* **19** A943
[3] Dogan P, Brandt O, Pfuller C, Lahnemann J, Jahn U, Roder C, Trampert A, Geelhaar L and Riechert H 2011 *Cryst. Growth Des.* **11** 4257
[4] Eddy C R, Nepal N, Hite J K and Mastro M A 2013 *J. Vac. Sci. Technol.* A **31** 058501
[5] Ling S C, Chao C L, Chen J R, Liu P C, Ko T S, Lu T C, Kuo H C, Wang S C, Cheng S J and Tsay J D 2010 *J. Cryst. Growth* **312** 1316
[6] Poppitz D, Lotnyk A, Gerlach J W and Rauschenbach B 2014 *Acta Mater.* **65** 98
[7] Yakimov E B, Polyakov A Y, Lee I H and Pearton S J 2018 *J. Appl. Phys.* **123** 115702
[8] Reshchikov M A, Albarakati N M, Monavarian M, Avrutin V and Morkoc H 2018 *J. Appl. Phys.* **123** 161520
[9] Massabuau F C P *et al* 2017 *Nano Lett.* **17** 4846
[10] Blenkhorn W E, Schulz S, Tanner D S P, Oliver R A, Kappers M J, Humphreys C J and Dawson P 2018 *J. Phys.: Condens. Matter* **30** 175303
[11] Cao L, Fu Q, Wu B and Xiong Y Q 2017 *J. Phys.: Condens. Matter* **29** 395302
[12] Elmaghraoui D, Triki M, Jaziri S, Munoz-Matutano G, Leroux M and Martinez-Pastor J 2017 *J. Phys.: Condens. Matter* **29** 105302
[13] Korona K P, Zytkiewicz Z R, Sobanska M, Sosada F E, Drozdz P A, Klosek K and Tchutchulashvili G 2018 *J. Phys.: Condens. Matter* **30** 315301
[14] Chen C, Song P F, Meng F C, Ou P F, Liu X Y and Song J 2018 *Nanotechnology* **29** 415501
[15] Liu L and Edgar J H 2002 *Mater. Sci. Eng.* R **37** 61
[16] Barchuk M, Holy V and Rafaja D 2018 *J. Appl. Phys.* **123** 161552
[17] Walde S, Brendel M, Zeimer U, Brunner F, Hagedorn S and Weyers M 2018 *J. Appl. Phys.* **123** 161551
[18] Mukherjee K, Reilly C H, Callahan P G and Seward G G E 2018 *J. Appl. Phys.* **123** 165701
[19] ElAfandy R T, Majid M A, Ng T K, Zhao L, Cha D and Ooi B S 2014 *Adv. Funct. Mater.* **24** 2305
[20] Yoshida S, Misawa S and Gonda S 1983 *Appl. Phys. Lett.* **42** 427
[21] Frajtag P, Samberg J P, El-Masry N A, Nepal N and Bedair S M 2011 *J. Cryst. Growth* **322** 27
[22] Li Q, Lin Y, Creighton J R, Figiel J J and Wang G T 2009 *Adv. Mater.* **21** 2416
[23] Zheleva T S, Smith S A, Thomson D B, Linthicum K J, Rajagopal P and Davis R F 1999 *J. Electron. Mater.* **28** L5
[24] Nakamura S *et al* 1998 *Appl. Phys. Lett.* **72** 211
[25] Nam O H, Bremser M D, Zheleva T S and Davis R F 1997 *Appl. Phys. Lett.* **71** 2638
[26] Colby R, Liang Z W, Wildeson I H, Ewoldt D A, Sands T D, Garcia R E and Stach E A 2010 *Nano Lett.* **10** 1568
[27] Jiang W K, Ehrentraut D, Downey B C, Kamber D S, Pakalapati R T, Do Yoo H and D'Evelyn M P 2014 *J. Cryst. Growth* **403** 18
[28] Chen C, Meng F C and Song J 2016 *J. Appl. Phys.* **119** 064302
[29] Chen C, Meng F C and Song J 2015 *J. Appl. Phys.* **117** 194301
[30] Giaremis S, Komninou P, Belabbas I, Chen J and Kioseoglou J 2018 *J. Appl. Phys.* **123** 244301
[31] Belabbas I, Chen J, Heggie M I, Latham C D, Rayson M J, Briddon P R and Nouet G 2016 *Model. Simul. Mater. Sci. Eng.* **24** 075001
[32] Bere A and Serra A 2002 *Phys. Rev.* B **65** 205323
[33] Weingarten N S 2018 *Comput. Mater. Sci.* **153** 409
[34] Weingarten N S and Chung P W 2013 *Scr. Mater.* **69** 311
[35] Zeng G S, Tan C K, Tansu N and Krick B A 2016 *Appl. Phys. Lett.* **109** 051602
[36] Zeng G S, Yang X F, Tan C K, Marvel C J, Koel B E, Tansu N and Krick B A 2018 *ACS Appl. Mater. Interfaces* **10** 29048
[37] Xin Y, Pennycook S J, Browning N D, Nellist P D, Sivananthan S, Omnes F, Beaumont B, Faurie J P and Gibart P 1998 *Appl. Phys. Lett.* **72** 2680
[38] Potin V, Ruterana P, Nouet G, Pond R C and Morkoc H 2000 *Phys. Rev.* B **61** 5587
[39] Liliental-Weber Z, Zakharov D, Jasinski J, O'Keefe M A and Morkoc H 2004 *Microsc. Microanal.* **10** 47
[40] Plimpton S 1995 *J. Comput. Phys.* **117** 1

[41] Hull D and Bacon D J 2001 *Introduction to Dislocations* (Amsterdam: Elsevier)

[42] Bulatov V and Cai W 2006 *Computer Simulations of Dislocations* (Oxford: Oxford University Press)

[43] Stillinger F H and Weber T A 1985 *Phys. Rev.* B **31** 5262

[44] Zhou X W, Ward D K, Martin J E, van Swol F B, Cruz-Campa J L and Zubia D 2013 *Phys. Rev.* B **88** 085309

[45] Zhou X W, Jones R E and Gruber J 2017 *Comput. Mater. Sci.* **128** 331

[46] Gruber J, Zhou X W, Jones R E, Lee S R and Tucker G J 2017 *J. Appl. Phys.* **121** 195301

[47] Chen C, Song P F, Meng F C, Ou P F, Liu X Y and Song J 2018 *Appl. Phys. Lett.* **113** 223501

[48] Chu K, Gruber J, Zhou X W, Jones R E, Lee S R and Tucker G J 2018 *Phys. Rev. Mater.* **2** 013402

[49] Shinoda W, Shiga M and Mikami M 2004 *Phys. Rev.* B **69** 134103

[50] Tuckerman M E, Alejandre J, Lopez-Rendon R, Jochim A L and Martyna G J 2006 *J. Phys. A: Math. Gen.* **39** 5629

[51] Yi M S, Lee H H, Kim D J, Park S J, Noh D Y, Kim C C and Je J H 1999 *Appl. Phys. Lett.* **75** 2187

[52] Nakamura S, Senoh M and Mukai T 1993 *Appl. Phys. Lett.* **62** 2390

[53] Ramesh C, Tyagi P, Yadav B S, Ojha S, Maurya K K, Kumar M S and Kushvaha S S 2018 *Mater. Sci. Eng. B* **231** 105

[54] Anderson P M, Hirth J P and Lothe J 2017 *Theory of Dislocations* (Cambridge: Cambridge University Press)

[55] Nord J, Albe K, Erhart P and Nordlund K 2003 *J. Phys.: Condens. Matter* **15** 5649